

Enhancing LGMD's Looming Selectivity for UAVs with Spatial-temporal Distributed Presynaptic Connection

Jiannan Zhao, *Member, IEEE*, Hongxin Wang, *Member, IEEE*, and Shigang Yue, *Member, IEEE*

Abstract—Collision detection is one of the most challenging tasks for Unmanned Aerial Vehicles (UAVs), especially for small or micro UAVs with limited computational power. In nature, fly insects with compact and simple visual systems demonstrate the amazing ability to navigating and avoid collision in a complex environment. A good example of this is locusts. Locusts avoid collision in a dense swarm relying on an identified vision neuron called Lobula Giant Movement Detector (LGMD) which has been modelled and applied on ground robots and vehicles. LGMD as a fly insect's visual neuron, is an ideal model for UAV collision detection. However, the existing models are inadequate in coping with complex visual challenges unique for UAVs. In this paper, we proposed a new LGMD model for flying robots considering distributed spatial-temporal computing for both excitation and inhibition to enhance the looming selectivity in flying scenes. The proposed model integrated recent discovered presynaptic connection types in biological LGMD neuron into a spatial-temporal filter with linear distributed interconnection. Systematic experiments containing quadcopter's first person view (FPV) flight videos demonstrated that the proposed distributed presynaptic structure can dramatically enhance LGMD's looming selectivity especially in complex flying UAV applications.

Index Terms—LGMD, UAV, looming, collision detection, presynaptic neural network.

I. INTRODUCTION

AUTONOMOUS flying robots or unmanned aerial vehicles (UAVs), especially small and micro aerial vehicles (MAVs), have demonstrated huge potential in serving human society recently with their flexible flyability. However, autonomous MAVs still cannot fly automatically for real service tasks, one of the reasons is that they have not been equipped with efficient collision detection capability. Traditional ways for collision detection, such as laser[1], ultrasonic[2], and Simultaneous Localization and Mapping(SLAM)[3] are either too computationally expensive or too dependent on objects' texture and physical characters such as absorbing and reflective ability, therefore are not ideal for MAVs. Vision sensors capture rich information of the real world yet are small and low power consuming. However, the abundant information demands efficient algorithms to extract features for specific tasks. For autonomous MAVs, their agile 3D movements yield much more background noise than ground robots. How

This work was supported in part by EU HORIZON 2020 Project STEP2DYNA under Grant 691154, in part by EU HORIZON 2020 Project ULTRACEPT under Grant 778062.

J. Doe and J. Doe are with Anonymous University.

Manuscript received April 19, 2005; revised August 26, 2015.

to discriminate crucial collision information for autonomous MAVs with limited computing resources is still challenging.

On the other hand, nature demonstrated thousands of successful collision detection solutions. For example, locusts' can fly agilely in a swarm of millions without collision. Their amazing collision sensitivity during agile flight relies on a visual looming detector found in their Lobula plate: the Lobula Giant Movement Detector (LGMD)[4]. The LGMD responds discriminately to looming obstacles and discards translating or receding interference, making it ideal for modelling in robotic platforms to detect head-on collisions.[5][6]. Some applicable LGMD inspired models have been studied, despite the precise structure and signal process in the LGMD neuron remain veiled. For example, Badia[7] used Reichard correlator[8] based EMD structure to extract expanding edges and applied the LGMD model for blimp collision detecting. Yue[9] enhanced the feature of LGMD with grouped excitation and decay. This model discriminates visual cues by laterally inhibiting neighbouring stimuli and feeding forward the output in a dynamic range with a global switch. It has been introduced as a robotic looming detector to mobile and hexapod robots[10][11][12], automatic drive scene[13][14], and a few UAV applications[15][16]. However, these LGMD models are still not, as the locust's LGMD neuron are, competent for agile flight in complex environments. Agile flight here refers to efficient flight with inevitable attitude or ego motion, which can cause severe background noise to the onboard vision sensor. An example of attitude motion caused camera movement is given in Fig. 1.

This issue brings a conundrum for LGMD based collision detector: the quadcopter needs to fly quickly to sustain efficiency, but this causes attitude motion and leads to LGMD false positive alarm. As demonstrated in In Fig. 2, the LGMD model[16][17] inevitably triggered false positive alarm when challenged with an FPV flight video of a small quadcopter in periods (ii) and (iii). These attitude motion are crucial for UAV's agile flights with efficiency and pan-tilts are not appropriate for power limited MAVs. To address this kind of conundrum for efficient flight application, the LGMD model needs to be significantly enhanced to cope with the agile flights while highlighting looming selectivity in dynamic and clustered environments.

Recent biological researches suggest that the retinotopic remapping and morphology in LGMD's dendritic fan play an important role in LGMD's looming selectivity[18]. Further study indicates that the presynaptic connection in LGMD

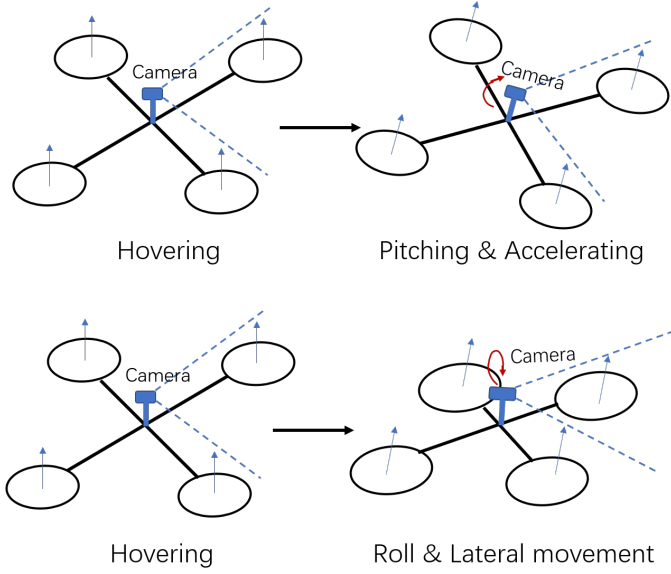


Fig. 1. UAVs attitude motion (quadcopter for example) during agile flight. Different from ground robots, UAV's agile flight is accompanied with attitude motions which will lead to ego-motion of the camera and cause severe background noise.

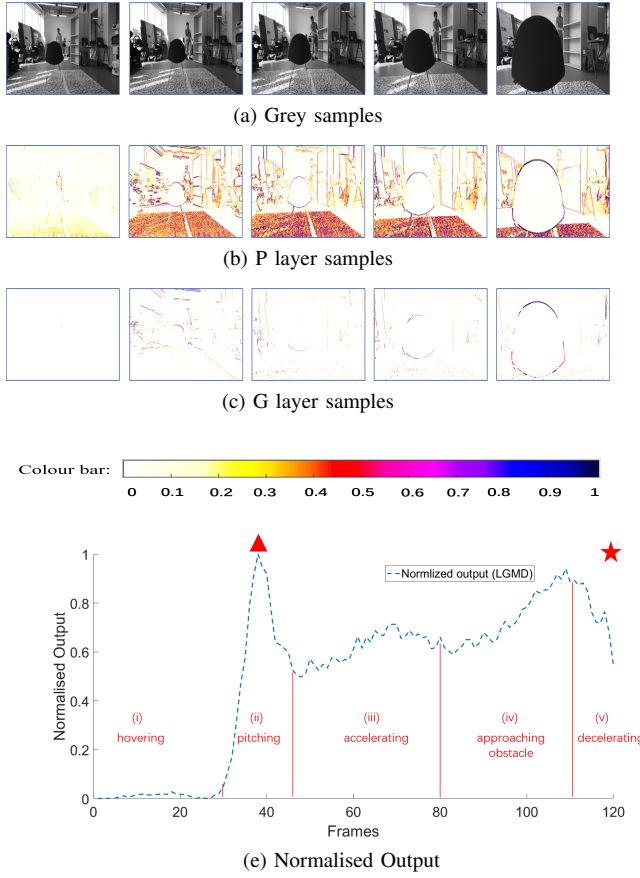


Fig. 2. LGMD Conundrum during agile flight of previous LGMD model[16]. Example frames are sampled at: 1,35,50,80,100. (a) Input grey samples of the FPV video. (b) and (c) P and G layer output transformed to heat-map. (d) colour bar (e) Normalised output MP of LGMD. Red triangle: the first peak of false positive, red star: the collision point. The flight experienced 4 periods: (i) hovering, (ii) pitching, (iii) accelerating, (iv) approaching obstacle (looming). Despite LGMD indeed filtered lots of noise, there remains many counters of surroundings in pitching and accelerating period.

is fine and distributed[19]. The distributed inhibitory[20] and excitatory[21] presynaptic interconnections contribute to LGMD's specific looming selectivity. These findings suggest that the presynaptic connection in the dendritic fan is exquisitely distributed and reciprocally connected, and this structure may lay the foundation of LGMD's discriminative response to looming. As far as we know, it is still not clear how presynaptic spatial-temporal distribution shaped the looming selectivity, and no computational model has been studied from this aspect. Inspired by these recent researches, we proposed the distributed presynaptic connection based LGMD model (D-LGMD) and systematically analysed how the spatial-temporal distribution contributes to LGMD's looming selectivity. Experimental results indicated that strong looming selectivity emerges after the cooperation of distributed excitatory and inhibitory linear reciprocal connection. The proposed presynaptic neural network model therefore acquired strong robustness in complex and dynamic visual scenes. The results of this research may not only provided a new UAV collision detecting solution for agile flights against complex backgrounds, but also revealed the significant recognition role a presynaptic neural network can play using distributed linear reciprocal connection.

In summary, the contribution of this paper is threefold:

- 1) Proposed a computational distributed presynaptic structure to enhance LGMD's looming selectivity. Within the presynaptic neural network, several recently observed reciprocal connection types (i.e. self-inhibition[20], lateral inhibition[4], distributed excitation[19]) are integrated with uniform description.
- 2) Systematically analysed the role of spacial-temporal distribution pattern of presynaptic connection in shaping LGMD's looming selectivity. Compared to previous computational models, D-LGMD's selectivity for looming is dramatically enhanced and flexibly tuned within the distributed presynaptic connection (DPC) layer.
- 3) Demonstrated the model's performance with real-flight UAV FPV colliding video. Solved LGMD's conundrum in complex dynamic scene by considerably enhancing the looming selectivity against other interfering stimuli.

The remainder of this paper is organized as follows. Section II, reviews related work on the LGMD model and UAV's collision detection. Section III, the proposed model is described in formulations. In Section IV, introduced experimental setup and materials. Section V, experiments are conducted to test the proposed model. Discussion is also given after the experiments. Finally, we conclude this paper in Section VI.

II. RELATED WORK

A. Traditional UAV's Collision Detection

Visual based collision detection for UAVs can be categorised into two types of strategies, one is to sense depth and react an escaping behaviour when an obstacle is at a given distance. This requires the controller to receive precise depth information about 3D environment in real time. There are many approaches to this, such as stereo-camera[22], LIDAR[23][24], optic flow based distance maintenance[25][26] and SLAM[3].

This type of methods are commonly used in UAVs with abundant power because they are comparatively robust. But these methods will not discriminate objects, in other words, it computes distance to every object in the whole FoV. And therefore, a redundant calculating power is involved in the process to have perception of 3D surroundings. It is interesting that in nature, only higher species or predators are likely to own depth based detector. Insects with small brains are unlikely to have perception of "depth", because their binocular overlapped field and spacing between their eyes are too small. Instead, they will sacrifice accuracy for efficiency by making use of basic monocular visual cues to sense collision or danger.

The second strategy uses a similar idea: to recognise obstacles with collision potential by monitoring their visual features. For example, within a single frame, it is applicable to recognise objects by feature points, and avoid the objects in the frontal area [27][28]. However, recognising the object is not necessary-and-sufficient for detecting collision, therefore, neither robust nor efficient. Additionally, based on the acknowledgement that image of looming objects will expand rapidly and non-linearly during collisions, some attempts have been made to detect the expansion of images on the retina for identifying objects that are approaching. for example, Mori[29] used SURF algorithm and template matching to detect relative-expansion of looming object. Al-Kaff[30] used sift algorithm and matching for relative-expansion. However, these traditional recognition methods are computational consuming in complex dynamic scenes.

B. Bio-inspired Collision Detection

Animals are evolved to arm efficient sensor system specialised for their living environments, and many insects are equipped with a designated visual system for flight. For example, optic flow is a fly-inspired method for visual perception. It has been studied in UAV's ego-motion estimation[31] and collision detection[25][32], but it is not appropriate for head-on collisions. As a complementary approach, optic flow can combine the idea of expansion detecting, which derived divergent optic flow based head-on collision detection[33][34].

LGMD is another bio-inspired collision detector, and it is known to be specialised for head-on looming objects [35]. Recent LGMD modelling researches such as Fu et al. proposed the on and off mechanism[36] to focus on dark looming objects, spiking frequency adaption mechanism[37] to feedback output MP with its derivative and FFI mediated inhibition[14] to adapt different background complexity. But these works was not validated in UAV applications. Our previous research demonstrated real time quadcopter collision avoidance with LGMD base collision detector[16][38]. In agile UAV flights, the complex dynamic image motion will generate spurious signal and contaminate the whole FoV of previous models. As a consequence, unsolvable false positive is yielded. Therefore, the existing LGMD model lacks robustness[39] even though Feed-forward Inhibition (FFI) is assumed to switch off response during self-rotation. Therefore, for more complex and dynamic applications, LGMD needs enhancement in discriminating looming stimuli from interfering signals.

C. Emerging Biological Findings about LGMD's Looming Selectivity

LGMD as a special single neuron has amazing recognition ability. Its looming selectivity largely comes from its dendritic fan[40], although the precise synaptic activation function remains controversial[41], recent biological researches thought highly of its retinotopic reciprocal connection in the dendritic area. It is observed that both excitatory and inhibitory presynaptic connections have overlapping portions[19][20], these results indicate that the dendrites receive fine distributed retinotopic projection from the photoreceptors and interact with neighbouring synapses before converging. The spatial-temporal race between excitation and inhibition likely lead to selective response for expanding over translating stimuli[5], and the distributed excitation would increase coherently expanding edges[21]. We put forth such a presynaptic layer which contains distributed excitatory and inhibitory reciprocal connection, and the connectivity is ruled by a uniform spatial-temporal distribution. As an LGMD-inspired collision detector, our work is different from Badia[42], which involved non-linear preprocessing of the image and multiplicative reciprocal connection. Our model extracts looming visual cues using linear reciprocal connection only. The looming selectivity first emerges after the retinotopic mapping (DPC layer), and before the postsynaptic inhibition (FFI). Compared to Yue[9], the looming selectivity in our model is flexibly tuned in the DPC layer using the spatial-temporal distribution and is of dramatically enhanced robustness in complex scenes. Compared to traditional visual methods, the proposed presynaptic filter is based on linear process towards luminance change, and therefore, is computationally efficient.

III. MODEL DESCRIPTION

This section presented the proposed distributed presynaptic connection based LGMD model (called D-LGMD for short) in formulations and described the virtual mechanism of filtering insignificant signals and eliciting looming cues.

A. Mechanism and schematic

As known from geometry, the image of an ideal looming object will experience a sharp nonlinear expanding near the collision point, both angular size and angular velocity of the image will increase non-linearly[43] as illustrated in Fig. 3. In a looming case, this type of non-linearly angular velocity is hardly reached by other source of visual stimuli like receding or translating objects. The proposed DPC layer forms a spatial-temporal filter to discriminate images' angular velocity on retina. It boosts fast expanding edges of looming objects and eliminates interfering stimuli caused by other visual sources. This is achieved by the combination of distributed excitation and the spatial-temporal race against presynaptic inhibition. Excitation of an object must win the race to reach the threshold in later layers. The faster the edge moves over the camera, the more excitatory units stand out. Once excitation of the coherently expanding edge exceed the offsetting impact of inhibition, excitatory units will mutually enhance because of the distributed reciprocal connection. The discriminative

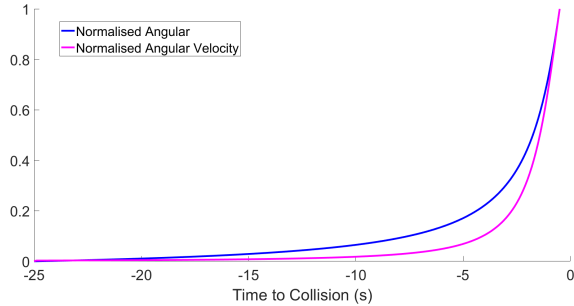


Fig. 3. Ideal object angular size and angular velocity via time during a looming process. Both curves are highly nonlinear, set a threshold on angle or angular velocity may be the strategy used by insects to identify collision cases[44]. This paper highlights nonlinear angular velocity for collision detection.

response to different angular velocity is tuned by the distribution functions which are pre-defined and consistent during computing process.

A schematic of the proposed D-LGMD model is presented in Fig. 4, D-LGMD can be described as 3 layers in the main signal stream, i.e. Photo receptors, distributed presynaptic reciprocal connection (DPC), grouping and decay (GD). Additionally, feed forward inhibition (FFI), a side pathway of postsynaptic inhibition[45], will mediate the GD threshold to regulate output MP in a dynamic range, so we call it FFI mediated grouping and decay (FFI-GD). And finally one single output terminal whose membrane potential (MP) reflects the threat level of collision in the whole FoV and will instruct downstream motion systems to avoid collisions. In general, there are 2 differences compared to previous LGMD models:

- 1) Excitatory and inhibitory interconnections are ruled by spatial-temporal distribution in DPC layer which pre-defined the preferred angular speed clearly. Therefore, D-LGMD can easily threshold out insignificant cues and acquired nonlinear response to looming objects. This non-linearity increased the robustness towards background noise and boost the quickly response to collision when looming object becomes prominent.
- 2) The side pathway, FFI will no longer switch off the output MP, but mediate the decay threshold after grouping. This new mechanism keeps the output MP in a dynamic range and enable the detector to remain sensitive in whole FoV changing scenes (e.g. attitude motion).

B. Photo-receptor layer

The first layer of the proposed model is photo receptor layer. As a motion sensitive visual model, the input layer extracts absolute luminance changes of each pixel:

$$P(x, y, t) = |L(x, y, t) - \int L(x, y, s) \delta(t - s - 1) ds| \quad (1)$$

where δ is the unit impulse function, $P(x, y, t)$ denotes the luminance change of pixel (x, y) at time t , and $L(x, y, t)$ denotes the luminance at time t . P layer responds to all image motion equally and does not discriminate backgrounds or foregrounds, translating, receding or looming.

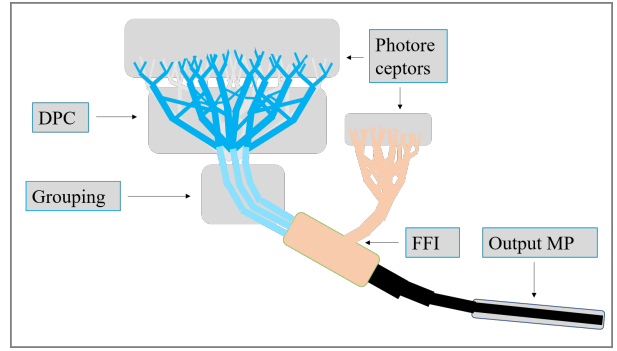


Fig. 4. D-LGMD neural model schematic. DPC:distributed presynaptic connection, FFI: feed forward inhibition, MP: membrane potential

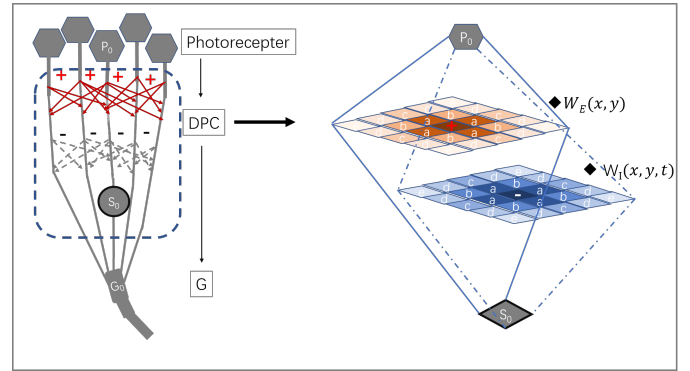


Fig. 5. DPC process illustration. "+" denotes excitation, "-" denotes inhibition. Both excitation and inhibition are mutually connected with neighbouring synapses, and the connectivity is ruled by distribution functions $W_E(x, y)$ and $W_I(x, y, t)$ (which are both symmetrical in spacial domain, and determined by distance, therefore, neighbouring synapses at symmetrical position have the same passing weights and latency).

C. DPC layer

After P layer, the image changes of whole FoV are extracted, only relatively moving edges are input to the next layer. DPC layer will enhance stimuli of looming or high speed objects and inhibit that of translating or backgrounds. Fig. 5 illustrated the schematic of DPC layer. The ability of discriminately responding to different visual stimuli sources is formed by reciprocal connected and interacted neural pathways including: interneuron excitation, interneuron inhibition and self-inhibition. Considering current researches of locust's LGMD neuron, the DPC layer will be consistent with the following assumed principles:

- 1) Containing both excitatory and inhibitory transmitter pathways[20].
- 2) The strength of connection tapers along the diameter from the root towards dendrite tip.[46][47].
- 3) Time race between excitation and inhibition is essential for image velocity selectivity.[4].

Thus we described the DPC layer with 2 distributions for excitatory and inhibitory pathways respectively, and integrated the time race between excitation and inhibition in distribution

functions:

$$E(x, y, t) = \iint P(x, y, t) W_E(x - u, y - v) du dv \quad (2)$$

$$I(x, y, t) = \iiint P(x, y, t) W_I(x - u, y - v, t - s) du dv ds \quad (3)$$

where $E(x, y, t)$ and $I(x, y, t)$ are excitation and inhibition at each pixel, W_E, W_I are the distribution function of excitation and inhibition respectively, considering principle 3), W_I contains distributions not only in spatial domain but also in temporal domain. consist with principle 2), Gaussian kernel is chosen to describe the two distributions in spatial domain:

$$\begin{cases} W_E(x, y) = G_{\sigma_E}(x, y) \\ W_I(x, y, t) = G_{\sigma_I}(x, y) \delta(t - h(x, y)) \end{cases} \quad (4)$$

Where σ_E, σ_I are standard differences of excitation and inhibition distribution, $h(x, y)$ is the temporal distribution function of inhibitory pathways. $h(x, y)$ is coordinates-determined and increased simultaneously with transmission distance:

$$h(x, y) = \alpha + \frac{1}{\beta + \exp(-\lambda^2(x^2 + y^2))} \quad (5)$$

where α, β, λ are time constants. An example of the temporal latency distribution is shown in Fig. 6 (note when $\alpha = \beta = \lambda = 0$, $h(t) = 1$). Time latency is necessary to form the spatial-temporal race between excitation and inhibition, which is well explained in Rind et. al[4]. Here we further put forth that the radial extending temporal distribution will sharpen the output curve because it produced a gradient for inhibition and selectively enhanced the barrier towards visual cues with relatively lower angular velocity. Fig. 7 illustrated this mechanism. With constant latency, Stimuli A at t_2 (lower angular velocity) in Fig. 7a is only inhibited by stimuli A at t_1 , which is similar to stimuli B (higher angular velocity). While with distributed latency, stimuli A in Fig. 7b will be replicatively inhibited by stimuli A at both t_1 and t_0 , and stimuli B will easily escape from inhibitory impact and stand out in later layer. After the distributed interconnection, the excitation and inhibition are integrated by linear summing (inhibition has opposite sign against excitation):

$$S(x, y, t) = E(x, y, t) - a \cdot I(x, y, t) \quad (6)$$

where $S(x, y, t)$ is the presynaptic sum corresponding to each pixel at time t , and a is the inhibition strength coefficient. Additionally, synapses stimuli will not be suppressed to negative, so a judgement equation is:

$$S(x, y, t) = \max[0, S(x, y, t)] \quad (7)$$

From the above formulations, the DPC layer formed a spatial-temporal filter, whose input is edges of moving objects. The latency between E and I pathway involves temporal information which cooperates with spacial distribution and forms the character of preferred angular velocity. Coherent excitations will mutually enhance, and must move faster to escape from the rejection band. Thus, only fast changing profiles of truly dangerous looming objects stand out after the "spatial-temporal filter", while the stimuli caused by slowly

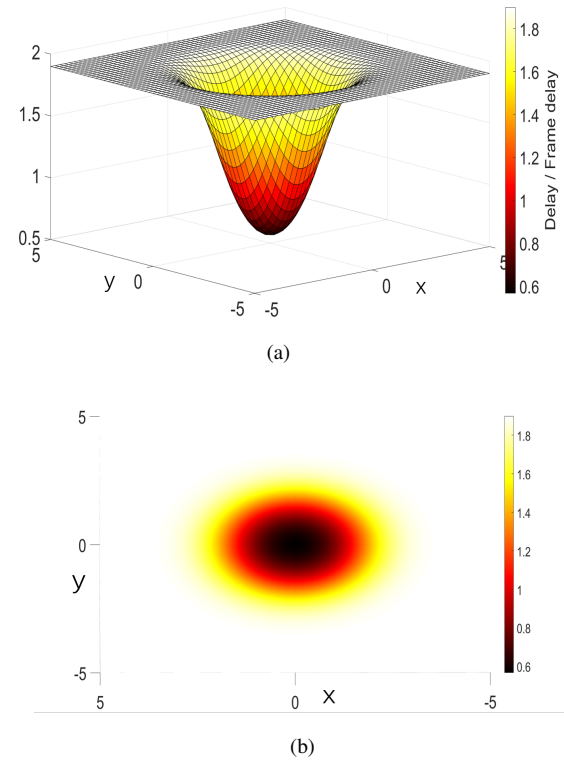


Fig. 6. $h(t)$ temporal latency distribution example. (a) kernel mesh, (b) top view. α, β, λ are set as $\alpha = -0.1, \beta = 0.5, \lambda = 0.7$.

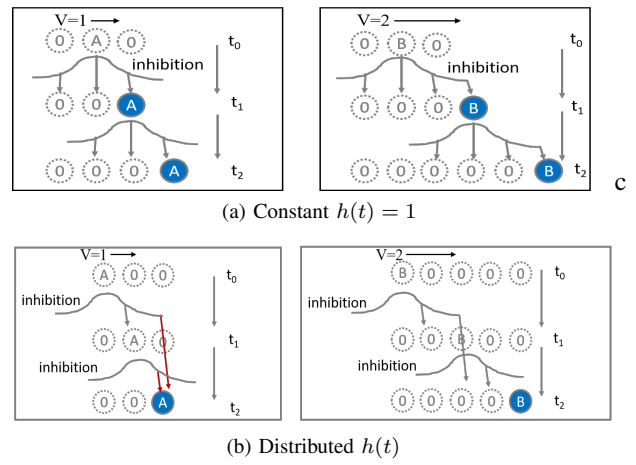


Fig. 7. Inhibitory impact comparison between constant time latency and radial distributed time latency. For example, stimuli A is moving slower than B, in case (a) with constant $h(t)$, stimuli B (the faster) received less inhibitory impact because of the spatial distribution. In (b), if we simply assume the latency distribution as 1 frame delay for 1 pixel distance and 2 frame delay for 2 pixel distance, with radial extending latency, inhibitory impact for stimuli A is replicative. At t_2 , stimuli A will receive main inhibitory impact from t_1 and secondary impact from t_0 . Contrarily, stimuli B will easily escape from the impact of t_0 and t_1 and stand out because of its higher angular speed. Therefore, the distributed $h(t)$ selectively enhanced the barrier to slowly changing stimuli.

translating objects or backgrounds are dramatically attenuated and will be further eliminated by threshold in the next layer. W_E , W_I , and $h(t)$ regulate the spatial-temporal distribution and rule the competition between excitation and inhibition, therefore, they shape the selectivity for objects with different angular velocity. Notably, Since the DPC layer discriminates angular velocity, if an object is close enough that it occupy huge area of the retina and translating at an extreme angular speed, it is also treated as a "dangerous target" that the model will respond an alarm. This character is also consistent with locust's behaviour experiments towards sudden translating[35].

D. FFI mediated grouping and decay

The output of DPC layer comes to grouping (G) layer and will be further enhanced if the excitation is clustered, and vice versa. G layer is introduced to this network in order to enhance expanded edges of looming object which is represented by clustered excitations[9]. This layer allows clusters of excitation from DPC layer easily pass to its corresponding G counterpart and provides a greater MP output. This mechanism is implemented by multiply the summation in DPC layer with a passing coefficient Ce :

$$G(x, y, t) = S(x, y, t) \cdot Ce(x, y, t) \quad (8)$$

Where $G(x, y, t)$ is the excitation corresponded to each dendritic cell in G layer and Ce is defined by a convolution operation from its neighbourhood given by:

$$Ce(x, y, t) = \iint_{\Omega} S(x - u, y - v, t) \cdot k dudv \quad (9)$$

where k is amplify constant and Ω is the neighbourhood area, in this paper, we set Ω as a 4×4 matrix. G layer is then followed by a threshold to filter out decayed signals:

$$\tilde{G}(x, y, t) = \begin{cases} G(x, y, t), & \text{if } G(x, y, t) \geq T_{de}(t) \\ 0, & \text{otherwise.} \end{cases} \quad (10)$$

The decay threshold $T_{de}(t)$ is mediated by the side pathway postsynaptic inhibition FFI, given by:

$$T_{de}(t) = \frac{FFI(t)}{n_{cell} \cdot m} \cdot T_0 \quad (11)$$

T_0 is the default maximal threshold, n_{cell} is the total number of pixels in a single frame, m is a constant coefficient. $FFI(t)$ is calculated by previous whole FoV image changes, given by:

$$FFI(t) = \iint |P(x, y, t - 1)| dx dy ds \quad (12)$$

The FFI-GD mechanism will no longer switch off the output MP, but mediate threshold level for single synaptic afferent according to luminance change in the whole FoV. This new mechanism further enhanced the coherently expanding edges of looming objects, kept the output MP in a dynamic range, and preserved the ability to work in complex and dynamic scenes.

TABLE I
CONSTANT PARAMETERS

| name | value | name | value |
|----------|-------|----------|-------|
| α | 0.3 | k | 1 |
| m | 0.4 | n_{sp} | 2 |
| T_0 | 0.5 | T_{MP} | 0.4 |

E. LGMD cell

The membrane potential (MP) of the LGMD cell $K(t)$ is finally calculated by summing results of whole FoV:

$$K(t) = \iint |\tilde{G}(x, y, t)| dx dy \quad (13)$$

If the MP $K(t)$ exceeds the threshold, a spike is produced:

$$S_f^{spike} = \begin{cases} 1, & \text{if } K(t) \geq T_{MP} \\ 0, & \text{otherwise.} \end{cases} \quad (14)$$

An impending collision is confirmed if successive spikes last consecutively no less than n_{sp} frames:

$$C_f^{LGMD} = \begin{cases} 1, & \text{if } \sum_{f=n_{sp}}^f S_f^{spike} \geq n_{sp} \\ 0, & \text{otherwise.} \end{cases} \quad (15)$$

The LGMD detector will generate an "avoid" command if the spikes last n_{sp} frames. Regular parameters are listed in Table I, these parameters are consistent in all the experiments in this paper.

IV. EXPERIMENTAL SETUP

The same quadcopter platform as described in [38] is used in this research. A webcam (OSMO Pocket) is used to record real-time FPV videos at 30 frame rate (1080P). Visual stimuli as input to the proposed neural network contain both simulated objects and real-time FPV videos. The simulation contains rendered scenes by Unity Engine, and basic approaching cubes generated by matlab. In real flight FPV videos, the webcam was glued on the quadcopter to capture real-time videos. Fig. 8 is the outlook of the quadcopter platform. The quadcopter was program-controlled to achieve: hovering, rotation, acceleration and uniform speed flight tasks. Different objects and surroundings are also considered in our experiments. The proposed model is running on a general laptop (with 2.5GHz Intel Core i5 CPU and 8GB memory) after prepared the above mentioned experimental materials.

V. EXPERIMENT RESULTS AND DISCUSSION

As mentioned in above sections, the proposed D-LGMD model lays a spatial-temporal filter to discriminate angular velocity and alarm as collision case when the output excitation exceeds a global threshold. In this sections, systematic experiments are conducted to analyse the character of D-LGMD in different scenes. Both qualitative comparison with previous LGMD model and quantitative parameter sensitivity experiments are presented. Both simulation and real flight FPV videos demonstrated the proposed D-LGMD has enhanced selectivity to looming especially during quadcopter's agile flight in complex scenes.



Fig. 8. Quadcopter Platform. The camera is glued on the quadcopter to capture FPV videos.

A. Characteristics of D-LGMD

To intuitively illustrate the layered network's signal process, we gave an example of Unity rendered scene and dissected the layered output in Fig. 9. The input scene contains 1 looming ball with uniform approaching speed and 4 capsules translating at 4 different speeds. P layer acquired luminance change without any selection, thus stimuli of all capsules and the looming ball were passed to the next layer. The DPC layer discriminated angular velocity and dramatically attenuated stimuli from translating. After that, G layer further filtered sparse or decayed signals and amplify the grouped excitation under the mediation of FFI.

Secondly, a simulated pure stimulus was input to compare the character between LGMD and D-LGMD. Fig. 10 showed the normalised output MP towards a looming and receding cube. In the looming case Fig. 10a, both LGMD and D-LGMD MP increased non-linearly as the cube approaching. Increasing of LGMD started gradually from the very beginning, while D-LGMD kept silent in the first period and sharply rose up near frame 15. This is because D-LGMD is more sensitive to preferred image angular velocity than other visual cues and therefore has better distinguish-ability when object is real dangerous than far away. Similarly, D-LGMD also showed better distinguish-ability towards receding objects, as can be seen from Fig. 10b. Similar to locust's LGMD neuron[5], when faced receding objects, D-LGMD's MP dropped to silent soon after the first activation. Nevertheless the LGMD model does not have such satisfactory ignorance for receding objects. This result indicates the proposed D-LGMD is relatively robust to receding interfering stimuli.

Furthermore, it is reasonable to define the "attenuation" for evaluating the impact of DPC layer as we considered the proposed DPC structure as a spatial temporal filter, which should have corresponding attenuation for images with different angular velocity. Here we define the "attenuation of DPC layer" as the log-transformed proportion between summation of DPC pixels and summation of input luminance changes:

$$\text{Attenuation}(t) = 10 \lg \left(\frac{\iint S(x, y, t) dx dy}{\iint P(x, y, t) dx dy} \right) \quad (16)$$

The attenuation is dependent on image's angular velocity. For example, Fig. 11 illustrated D-LGMD's attenuation change

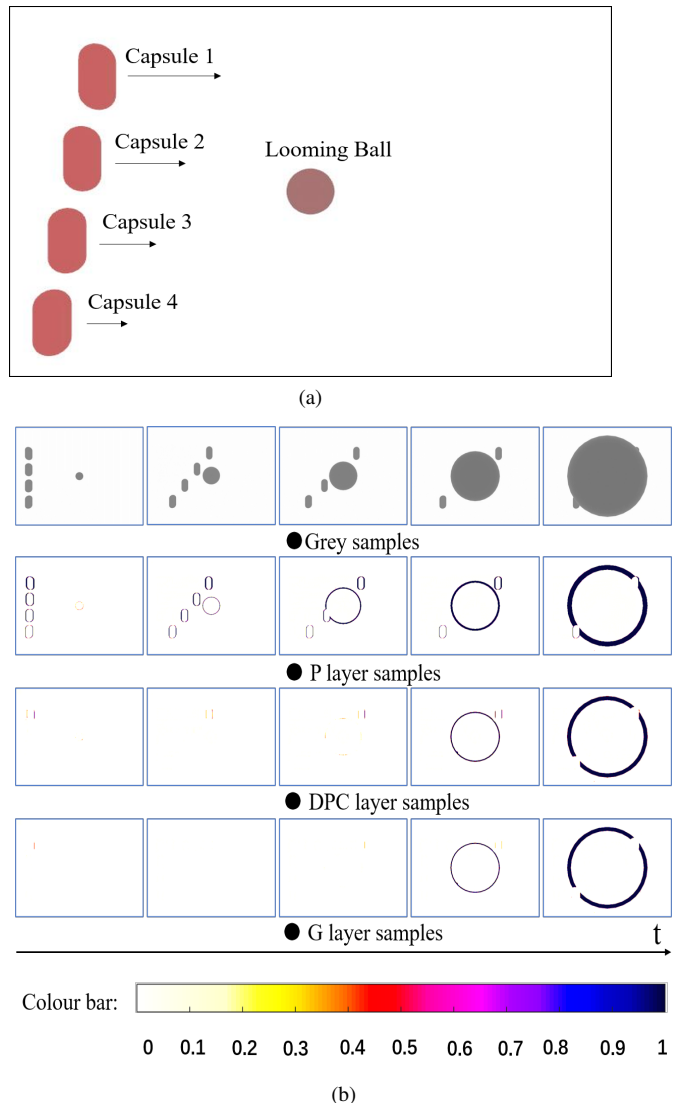


Fig. 9. Dissection of each layer's image process with Unity rendered input scene. For better resolution, P layer, S layer and G layer results are transformed to heat-map. (a) example input scene. (b) sampled frames of each layer.

during a looming process. The attenuation was strong for relative lower angular speed at the beginning, and rose up as the object getting closer. Compared to LGMD, D-LGMD showed stronger attenuation in start period and a sharper rise near the collision point, which means D-LGMD has stronger ability to discriminate the stimuli as the angular velocity of a looming object always increases non-linearly.

B. Parameter Sensitivity Analysis

D-LGMD's responding preference is determined by the spatial-temporal distribution. In this subsection, we discussed several crucial parameters for tuning this preference, including: inhibition strength a , standard deviations of excitation and inhibition distributions σ_E , σ_I , and time race coefficients α , β , λ . Parameters sets used in later experiments are listed in Table.II for comparison.

Fig. 12 showed how σ_E and σ_I tuned the attenuation towards different angular velocity. In general, D-LGMD has

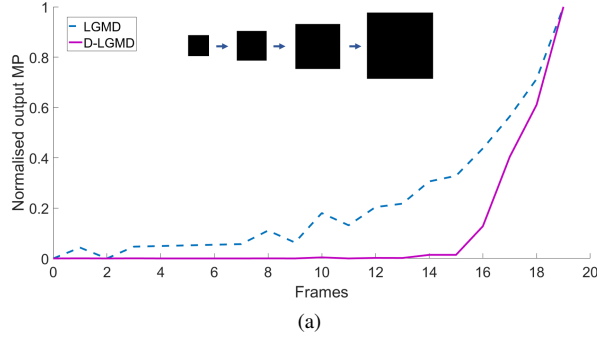
TABLE II
CRUCIAL PARAMETERS SETS

| sets | Temporal Distribution Parameters | | | Spatial Distribution Parameters | | | Other Parameters | |
|------|----------------------------------|------------|------------|---------------------------------|------------|-----|------------------|----------|
| | α | β | λ | σ_E | σ_I | a | T_0 | r |
| set1 | 0 | 0 | 0 | 0.35 | 1 | 1.5 | 0.5 | 4 |
| set2 | 0 | 0 | 0 | 0.35 | 1.8 | 1.5 | 0.5 | 4 |
| set3 | 0 | 0 | 0 | 0.35 | 2.5 | 1.5 | 0.5 | 4 |
| set4 | -0.1 | 0.5 | 0.7 | 0.35 | 1 | 1.5 | 0.5 | 4 |
| set5 | -0.1 | 0.5 | 0.7 | 0.35 | 1.8 | 1.5 | 0.5 | 4 |
| set6 | -0.1 | 0.5 | 0.7 | 0.35 | 2.5 | 1.5 | 0.5 | 4 |
| set7 | -0.1 | 0.5 | 0.7 | 1 | 5 | 1.5 | 0.5 | 4 |
| set8 | -0.1 | 0.5 | 0.7 | 1 | 5 | 1.5 | 0.5 | 6 |
| set9 | -0.1 | 0.5 | 0.7 | 1.5 | 5 | 1.5 | 0.5 | 6 |

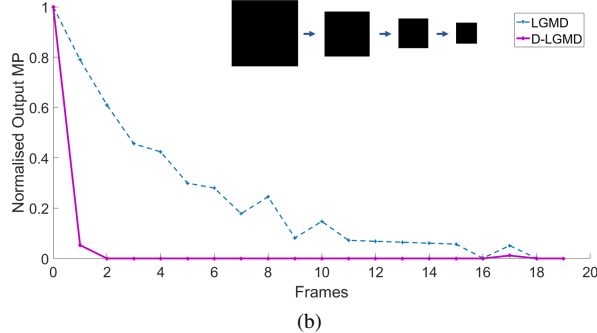
*r is calculating radius used when running on PC

TABLE III
DETAILS OF INPUT IMAGE SEQUENCES

| Image Sequence | Backgrounds Complexity | Attitude Motion | Object Texture | Collision Frame |
|----------------|------------------------|-----------------------------------|-------------------|-----------------|
| Group1 | Cluttered Indoor | Pitch, Accelerating | Pure Colour Chair | 120 |
| Group2 | Cluttered Indoor | Pitch, Accelerating, Decelerating | Gridding Pattern | 140 |
| Group3 | Rotation Indoor | Yaw | Notebook | 135 |
| Group4 | Simple Indoor | Take off, Pitch | Gridding Pattern | 210 |
| Group5 | Simple Indoor | Take off, Pitch | Carton | 196 |



(a)



(b)

Fig. 10. Comparative response for (a) looming and (b) receding object of LGMD and D-LGMD. Input stimuli are simulated image sequences of a looming or receding cube (sampled and stamped on the graph).

stronger attenuation for relatively lower speed object and vice versa. Specifically, increasing σ_I enhanced the inhibition towards stimuli with higher angular velocity, while increasing σ_E enhanced the coherently expanding edges of stimuli with higher angular velocity. Thus, tuning the spatial distribution parameter σ_E , σ_I makes it easy to select out preferred angular velocity and to identify image edges of dangerous objects.

Fig. 13 illustrated the impact of temporal distributed inter-

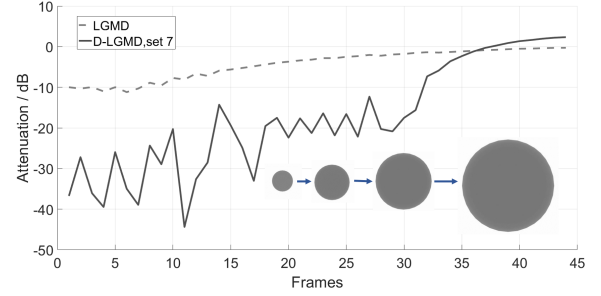


Fig. 11. Attenuation change during looming process (D-LGMD parameters: set 7). The input scene is a looming ball generated by Unity engine.

connection, which is tuned by time race coefficients α , β , λ . The radial distributed $h(t)$ sharpened the normalised output curve. Moreover, in Fig. 13a, the parameter sets with lower response in the beginning climbed over in looming period. This indicates that as parameter σ_I increasing, the performance getting better not only in the looming period (stronger output MP) but also has stronger attenuation when the stimuli is of lower angular velocity. This happened because the radial distributed time latency made it easier for stimuli of higher angular velocity to win the inhibition race as we explained in Fig. 7.

C. Performance in UAV FPV Videos

Finally, we challenged the model with recorded real flight videos. Various input scenes had been tested, including cluttered indoor environment, taking off, multi-axis attitude motion, self-rotation, acceleration and deceleration. Details of the experimental input sequences are listed in Table III.

Again, we challenged D-LGMD with the aforementioned conundrum (input sequences: Group 2), where LGMD produced unsolvable false positive in Fig. 2. The result of D-

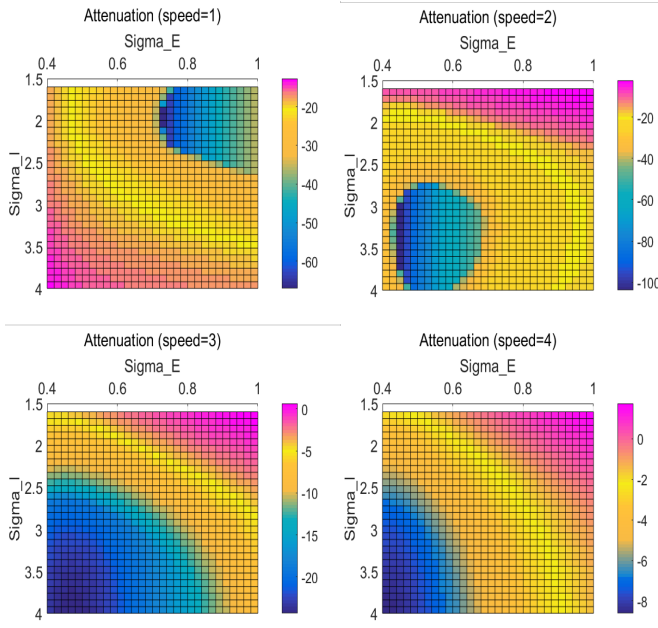


Fig. 12. Attenuation analyse towards different object speed. The input stimuli are translating cubes at 4 different speed: 1,2,3,4 (pixels/frame) which is equivalent to 9,18,27,36 ($^{\circ}/s$) in a 120° , 30 frame rate camera. Note the colour bar in each sub-picture represent different attenuation range. In general, the attenuation is much stronger for relatively lower speed object.

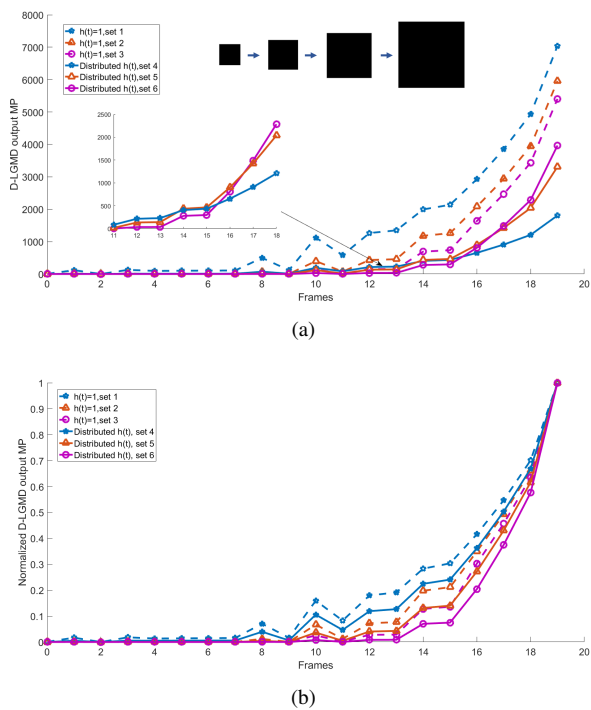


Fig. 13. Comparative experiments between distributed time delay and constant time delay. (a) Output MP, (b) Normalized MP

LGMD is presented in Fig. 14. Note when LGMD model faced the first false positive, D-LGMD model remains almost silent, and kept a indistinctive level during accelerating also. Before the collision point, D-LGMD responded a quick activation, and the curve climbed up sharply to peak. The FFI-GD mechanism further eliminated noisy spikes and smoothed the curve.

Then we tested the model with the same scene but changed the object with a different pattern, as shown in Fig. 15(input sequences: Group 2). We also discussed typical parameter sets in this complex scene. The selected parameter sets were not optimised but very typical: Set3 rarely has excitatory distribution and the temporal latency is constant. Set6 involved distributed latency. Set7 has wider excitatory and inhibitory distribution kernel, but restricted the calculating radius as 4 ($r = 4$ cannot fully reflect the kernel). Set8 extended the calculating radius to 6 and made full use of the convolution kernel. The results clearly showed the different impact of parameters: Set 3 and set 7 remains a small response near frame 40 (pitching). This small response is eliminated in set 6, 8 when added temporal distribution or increased calculating radius respectively. Set 3 and 6 were largely affected by the decelerating process and leads to a drop down near frame 120. This indicate that these two sets (with smaller σ_E , σ_I and calculating radius r) may not has consistent performance when faced decelerating looming object.

And also, D-LGMD worked well in relative simple environment (Fig16 and Fig17). Both LGMD and D-LGMD were available to detect collision in these simple scenes. However, LGMD results remained several small peaks during attitude motion. The attenuation curves reflected the difference from another aspect: D-LGMD showed strong discrimination in different periods, strong attenuation is observed after taking off, and the attenuation curve prominently rose up during the looming periods.

Additionally, we challenged the model during self-rotation (yaw motion). Results in Fig. 18 indicated D-LGMD preserved the ability to discriminate looming cue during rotation flight.

D. Computation Complexity

The computational complexity of DPC layer is essentially determined by the 2D convolutions of the input image sequences with W_E and W_I (equation(2) and (3)), which can be implemented in $O(2r^2mn)$ times for an $m \times n$ input image and $r \times r$ size kernel. In other words, the computation complexity is mainly determined by the calculating radius and input image size. Obviously, calculating radius should cover the significant area of the kernel to present its character. As discussed above, filtering faster background noise requires a "larger" kernel but also leads to increasing computational complexity. The good news is, reducing input image size (as long as the image preserved important features of looming process) would increase the distinguishability to looming case because D-LGMD discriminates image velocity by pixel interconnections and resizing the input image size also redefined the kernel's impact area corresponding to the real scene. Therefore, D-LGMD can work with extreme low resolution input as reducing image size makes the kernel cover

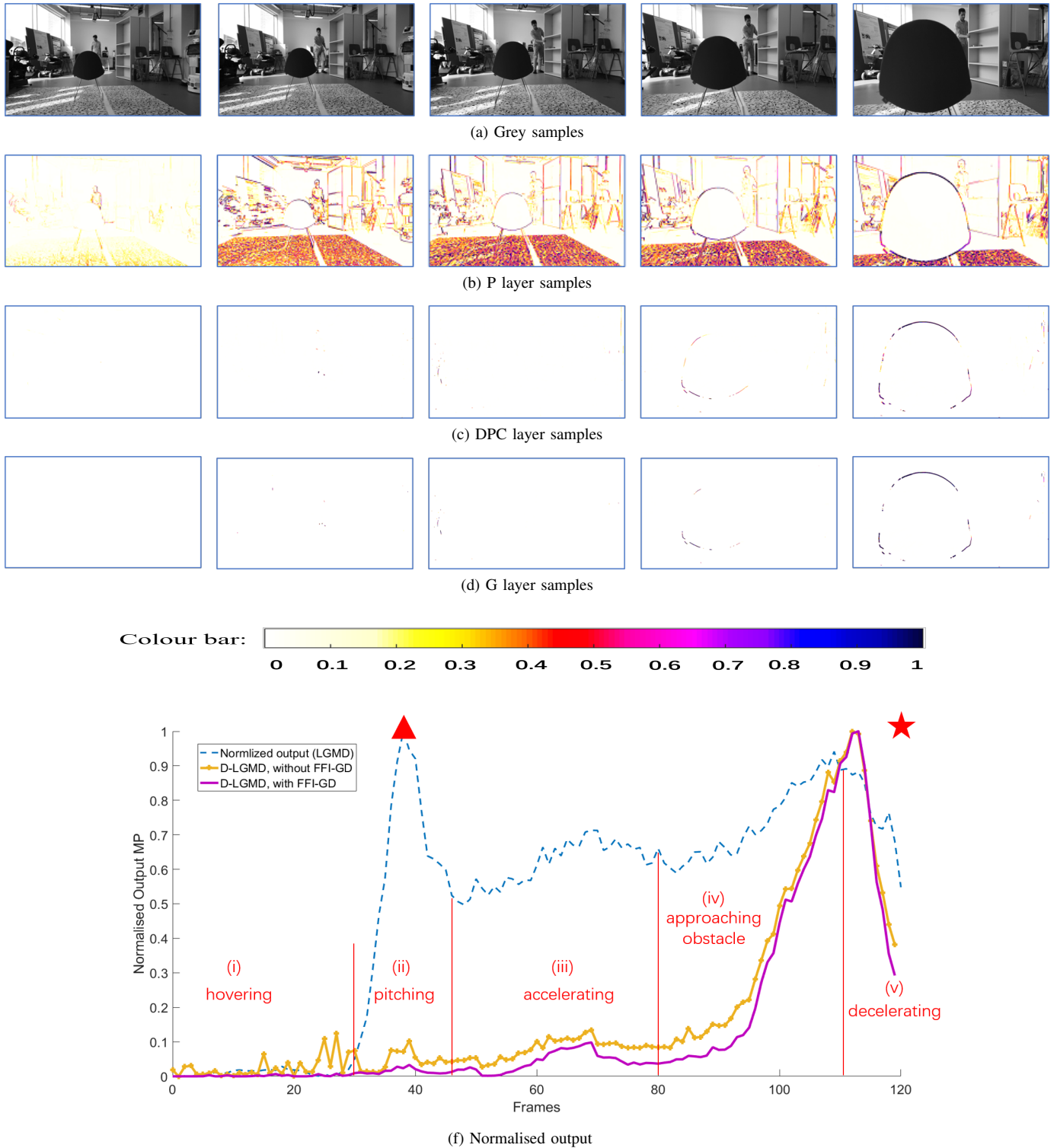


Fig. 14. D-LGMD response of the aforementioned conundrum as a comparison with Fig. 2 (the same input sequences: Group 2, D-LGMD parameters: set9, example frames are sampled at: 1,35,50,80,100). Layered results are dissected and transformed into heat maps. The flight experienced 5 periods: (i) hovering, (ii) pitching, (iii) accelerating, (iv) approaching obstacle (looming), (v) Program controlled decelerating (to avoid hardware damage). Red triangle: first false positive peak of LGMD result, red star: the collision point. The false positive of LGMD model during period (ii) and (iii) is eliminated in D-LGMD results.

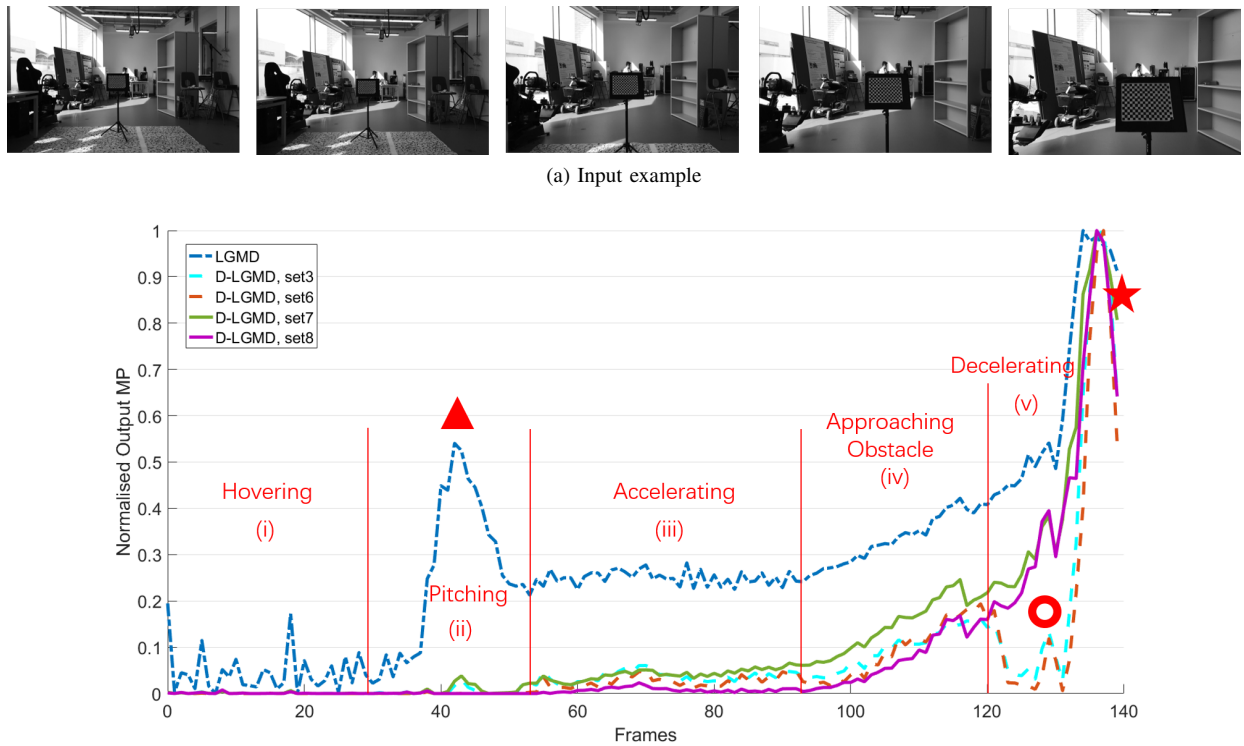


Fig. 15. Complex indoor flight (input sequences: Group 2). Collision occurred at frame 140. Pitching and accelerating started at frame 40. Near frame 125 (the red circle), the quadcopter was program controlled to decelerate (in order to reduce physical damage). Red triangle: first false positive in LGMD model, red circle: unexpected negative during program controlled decelerating near the collision point, red star: the collision point. Set 3 and set 7 remains a small response near frame 40 (pitching). This small response is eliminated in set 6, 8 when added temporal distribution or increased calculating radius respectively. Set 3 and 6 were largely affected by the decelerating process and leads to a drop down near frame 120. This indicate that these two sets (with smaller σ_E , σ_I and calculating radius r) may not has consistent performance when faced decelerating looming object.

a larger area and enhanced the barrier to background noise. Here we systematically analysed the relationship between the distinguishability to looming, calculating radius, input image size and computational complexity by 200 trials running on PC. The results are listed in Table IV. The distinguishability (DA) is quantised as the average output MP at peak point divided by average MP at false positive point (i.e. Fig.14f): $DA = \text{average}(MP_{\text{peak}}) / \text{average}(MP_{\text{false-positive}})$. Theoretically, when $DA \leq 1$, it is impossible to select out looming cues from dynamic backgrounds during agile flight. From experimental experience, if $DA > 10$, the model is very competent at filtering the interfering stimuli and is foreseeable to be robust against various scenes. As input size ranging from default to 0.1 times, DA was first increased and then decreased. For all the calculating radius, the best DA results existed when input images were resized to 0.25 times. The proposed model showed satisfactory DA results even with extreme low resolution input images. The only insufficient DA was generated when computing the default size (1080P) input with $r = 2$, where $DA = 3.87$ means the looming case is distinguishable but not prominent enough.

VI. CONCLUSION

The UAV's agile flight brings camera's ego-motion and leads to confusing false positive in visual motion based collision detecting algorithms. Inspired by state-of-the-art researches of locust's LGMD neuron, this paper proposed a

computational presynaptic neural network model as a solution for collision detection in agile UAV flight applications. The detecting mechanism is targeted to looming object's nonlinear growing image angular velocity on the retina. Our model integrates distributed excitation and distributed time latency with distribution functions and forms a spatial-temporal filter to selectively build the barrier against translating and background stimuli that has relatively lower image angular velocity. Using FFI-GD mechanism, D-LGMD preserved collision detecting ability during UAV's attitude motion including pitching, accelerating, decelerating and self-rotation. Systematic experiments demonstrated the proposed method has dramatically enhanced distinguishability to looming objects against background noise caused by agile flight and therefore showed strong robustness in complex dynamic visual scenes. Moreover, the proposed method worked well even with extreme small input image size. Compacting the size of input images did not harm the performance but increased the distinguishability towards looming case. This character is superior when energy consumption is critical such as embedded systems and MAVs.

ACKNOWLEDGMENT

The authors would like to thank...

REFERENCES

- [1] A. Bachrach, R. He, and N. Roy, "Autonomous flight in unknown indoor environments," *International Journal of Micro Air Vehicles*, vol. 1, no. 4, pp. 217–228, 2009.

TABLE IV
COMPUTATION COMPLEXITY

| Calculating Radius (r) | Image resizing | Distinguishability (DA) | O (DPC) | PC Run Time (10 times average) |
|------------------------|----------------|-------------------------|--|--------------------------------|
| 6 | default | 249.33 | $2 \times 6^2 \times 1920 \times 1080$ | 9.18s |
| 6 | 0.5 | 9789.28 | $2 \times 6^2 \times 960 \times 540$ | 2.75s |
| 6 | 0.25 | > 10000 | $2 \times 6^2 \times 480 \times 270$ | 1.06s |
| 6 | 0.1 | > 10000 | $2 \times 6^2 \times 192 \times 108$ | 0.75s |
| 6 | 0.02 | 1354.10 | $2 \times 6^2 \times 38 \times 22$ | 0.60s |
| 4 | default | 33.44 | $2 \times 4^2 \times 1920 \times 1080$ | 8.71s |
| 4 | 0.5 | 691.20 | $2 \times 4^2 \times 960 \times 540$ | 2.54s |
| 4 | 0.25 | 4579.40 | $2 \times 4^2 \times 480 \times 270$ | 0.98s |
| 4 | 0.1 | 105.33 | $2 \times 4^2 \times 192 \times 108$ | 0.70s |
| 4 | 0.02 | 184.54 | $2 \times 4^2 \times 38 \times 22$ | 0.59s |
| 3 | default | 9.1 | $2 \times 3^2 \times 1920 \times 1080$ | 8.70s |
| 3 | 0.5 | 96.75 | $2 \times 3^2 \times 960 \times 540$ | 2.53s |
| 3 | 0.25 | 1227.60 | $2 \times 3^2 \times 480 \times 270$ | 0.97s |
| 3 | 0.1 | 36.13 | $2 \times 3^2 \times 192 \times 108$ | 0.67s |
| 3 | 0.02 | 76.06 | $2 \times 3^2 \times 38 \times 22$ | 0.57s |
| 2 | default | 3.87 | $2 \times 2^2 \times 1920 \times 1080$ | 8.67s |
| 2 | 0.5 | 11.09 | $2 \times 2^2 \times 960 \times 540$ | 2.49s |
| 2 | 0.25 | 32.29 | $2 \times 2^2 \times 480 \times 270$ | 0.95s |
| 2 | 0.1 | 11.76 | $2 \times 2^2 \times 192 \times 108$ | 0.66s |
| 2 | 0.02 | 18.47 | $2 \times 2^2 \times 38 \times 22$ | 0.57s |

Note: DA is defined as the average output MP at peak point divided by average MP at false positive point (i.e. Fig.14f)

DA = $\text{average} (MP_{\text{peak}}) / \text{average} (MP_{\text{false-positive}})$. Parameters used are consistent with set 7 in TABLE II (except r). Input scene is Group1 in Table III. PC Run Time contains the whole process of loading 120 frames of input images and running the model.

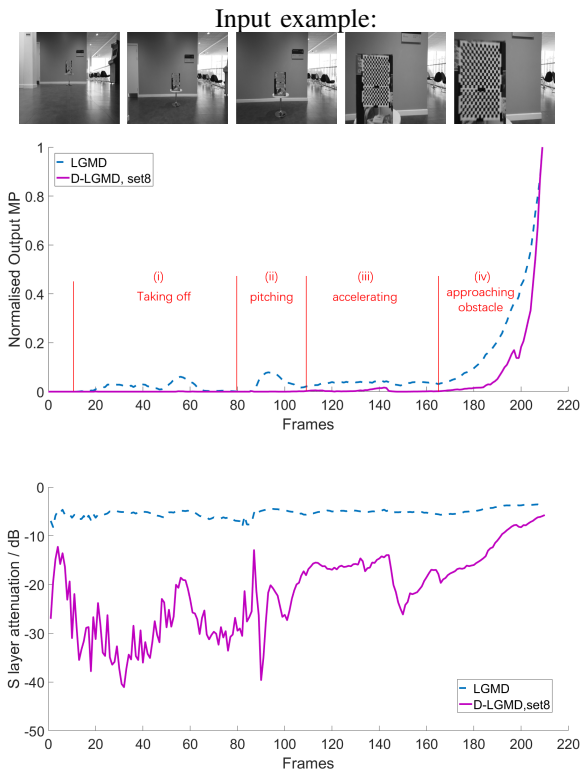


Fig. 16. Simple indoor flight (input sequences: Group 4). Collision occurred near frame 210, attitude motion periods are annotated on normalised result.

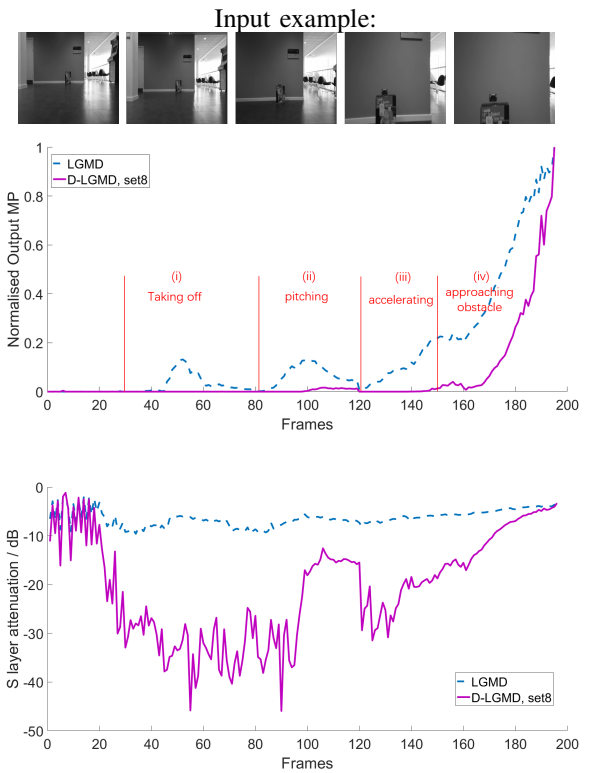


Fig. 17. Simple indoor flight2 (input sequences: Group 5). Collision occurred near frame 198, attitude motion periods are annotated on normalised result.

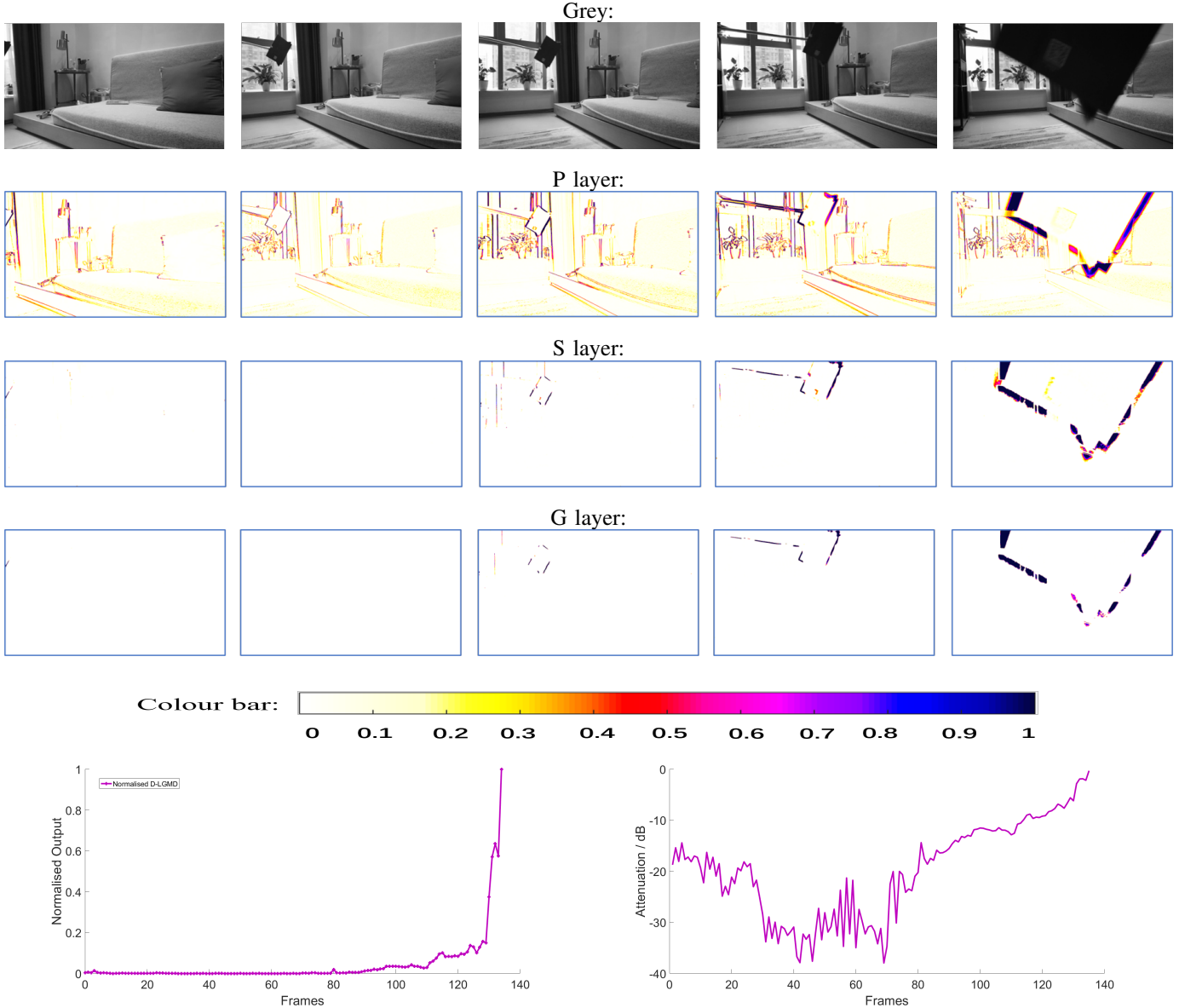


Fig. 18. Detecting Collision during self-rotation (input sequences: Group 3). The quadcopter was program controlled to rotate at $10^\circ/s$. Example images were sampled at 1,70,100,116,131. The attenuation curve showed strong inhibition during rotation and vice versa when object getting close.

- [2] X. Yu and Y. Zhang, "Sense and avoid technologies with applications to unmanned aircraft systems: Review and prospects," *Progress in Aerospace Sciences*, vol. 74, pp. 152–166, 2015.
- [3] B. Steder, G. Grisetti, C. Stachniss, and W. Burgard, "Visual slam for flying vehicles," *IEEE Transactions on Robotics*, vol. 24, no. 5, pp. 1088–1093, 2008.
- [4] F. C. Rind and D. Bramwell, "Neural network based on the input organization of an identified neuron signaling impending collision," *Journal of Neurophysiology*, vol. 75, no. 3, pp. 967–985, 1996.
- [5] F. C. Rind, "Motion detectors in the locust visual system: From biology to robot sensors," *Microscopy Research & Technique*, vol. 56, no. 4, pp. 256–269, 2002.
- [6] Q. Fu, H. Wang, C. Hu, and S. Yue, "towards computational models and applications of insect visual systems for motion perception: A review," *Artificial life*, vol. 25, no. 3, pp. 263–311, 2019.
- [7] S. Bermudez, i Badia, P. Pyk, and P. F. Verschure, "A fly-locust based neuronal control system applied to an unmanned aerial vehicle: the invertebrate neuronal principles for course stabilization, altitude control and collision avoidance," *International Journal of Robotics Research*, vol. 26, no. 7, pp. 759–772, 2007.
- [8] M. Egelhaaf and W. Reichardt, "Dynamic response properties of movement detectors: theoretical analysis and electrophysiological investigation in the visual system of the fly," *Biological Cybernetics*, vol. 56, no. 2-3, pp. 69–87, 1987.
- [9] S. Yue and F. C. Rind, "Collision detection in complex dynamic scenes using an Igmd-based visual neural network with feature enhancement," *IEEE transactions on neural networks*, vol. 17, no. 3, pp. 705–716, 2006.
- [10] P. Čížek, P. Milička, and J. Faigl, "Neural based obstacle avoidance with cpg controlled hexapod walking robot," in *2017 International Joint Conference on Neural Networks (IJCNN)*. IEEE, 2017, pp. 650–656.
- [11] C. Hu, F. Arvin, and S. Yue, "Development of a bio-inspired vision system for mobile micro-robots," in *Joint IEEE International Conferences on Development and Learning and Epigenetic Robotics*. IEEE, 2014, pp. 81–86.
- [12] C. Hu, F. Arvin, C. Xiong, and S. Yue, "A bio-inspired embedded vision system for autonomous micro-robots: the Igmd case," *IEEE Transactions on Cognitive and Developmental Systems*, vol. PP, no. 99, pp. 1–1, 2016.
- [13] S. Yue and F. C. Rind, "Postsynaptic organisations of directional selective visual neural networks for collision detection," *Neurocomputing*, vol. 103, pp. 50–62, 2013.
- [14] Q. Fu, N. Bellotto, H. Wang, F. C. Rind, H. Wang, and S. Yue, "A visual neural network for robust collision perception in vehicle driving

scenarios,” in *IFIP International Conference on Artificial Intelligence Applications and Innovations*. Springer, 2019, pp. 67–79.

[15] L. Salt, D. Howard, G. Indiveri, and Y. Sandamirskaya, “Parameter optimization and learning in a spiking neural network for uav obstacle avoidance targeting neuromorphic processors,” *IEEE Transactions on Neural Networks and Learning Systems*, 2019.

[16] J. Zhao, C. Hu, C. Zhang, Z. Wang, and S. Yue, “A bio-inspired collision detector for small quadcopter,” in *2018 International Joint Conference on Neural Networks (IJCNN)*. IEEE, 2018, pp. 1–7.

[17] S. Yue, F. C. Rind, M. S. Keil, J. Cuadri, and R. Stafford, “A bio-inspired visual collision detection mechanism for cars: Optimisation of a model of a locust neuron to a novel environment,” *Neurocomputing*, vol. 69, no. 13, pp. 1591–1598, 2006.

[18] R. B. Dewell and F. Gabbiani, “Active membrane conductances and morphology of a collision detection neuron broaden its impedance profile and improve discrimination of input synchrony,” *Journal of neurophysiology*, vol. 122, no. 2, pp. 691–706, 2019.

[19] Y. Zhu and F. Gabbiani, “Fine and distributed subcellular retinotopy of excitatory inputs to the dendritic tree of a collision-detecting neuron,” *Journal of neurophysiology*, vol. 115, no. 6, pp. 3101–3112, 2016.

[20] F. C. Rind, S. Wernitznig, P. Pölt, A. Zankel, D. Gütl, J. Sztarker, and G. Leitinger, “Two identified looming detectors in the locust: ubiquitous lateral connections among their inputs contribute to selective responses to looming objects,” *Scientific reports*, vol. 6, p. 35525, 2016.

[21] Y. Zhu, R. B. Dewell, H. Wang, and F. Gabbiani, “Pre-synaptic muscarinic excitation enhances the discrimination of looming stimuli in a collision-detection neuron,” *Cell reports*, vol. 23, no. 8, pp. 2365–2378, 2018.

[22] S. Hrabar, G. S. Sukhatme, P. Corke, K. Usher, and J. Roberts, “Combined optic-flow and stereo-based navigation of urban canyons for a uav,” in *2005 IEEE/RSJ International Conference on Intelligent Robots and Systems*. IEEE, 2005, pp. 3309–3316.

[23] C. Richter, W. Vega-Brown, and N. Roy, “Bayesian learning for safe high-speed navigation in unknown environments,” in *Robotics Research*. Springer, 2018, pp. 325–341.

[24] C. Richter, A. Bry, and N. Roy, “Polynomial trajectory planning for aggressive quadrotor flight in dense indoor environments,” in *Robotics Research*. Springer, 2016, pp. 649–666.

[25] C. Sabo, A. Cope, K. Gurny, E. Vasilaki, and J. Marshall, “Bio-inspired visual navigation for a quadcopter using optic flow,” *AIAA Infotech@ Aerospace*, vol. 404, 2016.

[26] J. Keshavan, G. Gremillion, H. Alvarez-Escobar, and J. S. Humbert, “Autonomous vision-based navigation of a quadrotor in corridor-like environments,” *International Journal of Micro Air Vehicles*, vol. 7, no. 2, pp. 111–123, 2015.

[27] W. G. Aguilar, V. P. Casaliglla, and J. L. Pólit, “Obstacle avoidance based-visual navigation for micro aerial vehicles,” *Electronics*, vol. 6, no. 1, p. 10, 2017.

[28] R. Carloni, V. Lippiello, M. D’auria, M. Fumagalli, A. Y. Mersha, S. Stramigioli, and B. Siciliano, “Robot vision: Obstacle-avoidance techniques for unmanned aerial vehicles,” *IEEE Robotics & Automation Magazine*, vol. 20, no. 4, pp. 22–31, 2013.

[29] T. Mori and S. Scherer, “First results in detecting and avoiding frontal obstacles from a monocular camera for micro unmanned aerial vehicles,” in *2013 IEEE International Conference on Robotics and Automation*. IEEE, 2013, pp. 1750–1757.

[30] A. Al-Kaff, F. García, D. Martín, A. De La Escalera, and J. M. Armingol, “Obstacle detection and avoidance system based on monocular camera and size expansion algorithm for uavs,” *Sensors*, vol. 17, no. 5, p. 1061, 2017.

[31] A. Briod, J. C. Zufferey, and D. Floreano, “A method for ego-motion estimation in micro-hoovering platforms flying in very cluttered environments,” *Autonomous Robots*, vol. 40, no. 5, pp. 789–803, 2016.

[32] J. R. Serres and F. Ruffier, “Optic flow-based collision-free strategies: From insects to robots,” *Arthropod structure & development*, vol. 46, no. 5, pp. 703–717, 2017.

[33] J. C. Zufferey and D. Floreano, “Fly-inspired visual steering of an ultralight indoor aircraft,” *IEEE Transactions on Robotics*, vol. 22, no. 1, pp. 137–146, 2006.

[34] J.-L. Stevens and R. Mahony, “Vision based forward sensitive reactive control for a quadrotor vtol,” in *2018 IEEE/RSJ International Conference on Intelligent Robots and Systems (IROS)*. IEEE, 2018, pp. 5232–5238.

[35] F. C. Rind and P. J. Simmons, “Orthopteran demd neuron: a reevaluation of responses to moving objects. i. selective responses to approaching objects,” *Journal of Neurophysiology*, vol. 68, no. 5, pp. 1654–1666, 1992.

[36] Q. Fu, C. Hu, J. Peng, F. C. Rind, and S. Yue, “A robust collision perception visual neural network with specific selectivity to darker objects,” *IEEE Transactions on Cybernetics*, 2019.

[37] Q. Fu, C. Hu, J. Peng, and S. Yue, “Shaping the collision selectivity in a looming sensitive neuron model with parallel on and off pathways and spike frequency adaptation,” *Neural Networks*, vol. 106, pp. 127–143, 2018.

[38] J. Zhao, X. Ma, Q. Fu, C. Hu, and S. Yue, “An Igmd based competitive collision avoidance strategy for uav,” in *IFIP International Conference on Artificial Intelligence Applications and Innovations*. Springer, 2019, pp. 80–91.

[39] A. Beyeler, J.-C. Zufferey, and D. Floreano, “Vision-based control of near-obstacle flight,” *Autonomous robots*, vol. 27, no. 3, p. 201, 2009.

[40] Graham and Lyle, “How not to get caught,” *Nature Neuroscience*, vol. 5, no. 12, pp. 1256–1257, 2002.

[41] F. Gabbiani, G. Laurent, N. Hatsopoulos, and H. G. Krapp, “The many ways of building collision-sensitive neurons,” *Trends in neurosciences*, vol. 22, no. 10, pp. 437–438, 1999.

[42] S. Bermudez i Badia, P. Pyk, and P. F. Verschure, “A fly-locust based neuronal control system applied to an unmanned aerial vehicle: the invertebrate neuronal principles for course stabilization, altitude control and collision avoidance,” *The International Journal of Robotics Research*, vol. 26, no. 7, pp. 759–772, 2007.

[43] F. Gabbiani, H. G. Krapp, and G. Laurent, “Computation of object approach by a wide-field, motion-sensitive neuron,” *Journal of Neuroscience*, vol. 19, no. 3, pp. 1122–1141, 1999.

[44] ———, “Computation of object approach by a wide-field, motion-sensitive neuron,” *Journal of Neuroscience*, vol. 19, no. 3, pp. 1122–1141, 1999.

[45] R. D. Santer, R. Stafford, and F. C. Rind, “Retinally-generated saccadic suppression of a locust looming-detector neuron: investigations using a robot locust,” *Journal of The Royal Society Interface*, vol. 1, no. 1, pp. 61–77, 2004.

[46] H. Cuntz, A. Borst, and I. Segev, “Optimization principles of dendritic structure,” *Theoretical Biology and Medical Modelling*, vol. 4, no. 1, p. 21, 2007.

[47] H. Cuntz, F. Forstner, A. Borst, and M. Häusser, “One rule to grow them all: a general theory of neuronal branching and its practical application,” *PLoS computational biology*, vol. 6, no. 8, p. e1000877, 2010.

Jiannan Zhao Biography text here.

PLACE
PHOTO
HERE

Hongxin Wang Biography text here.

Shigang Yue Biography text here.